From bell-shapes to pyramids: a continuum model for self-assembled quantum dot growth

M. D. Korzec* P. L. Evans†

July 15, 2009

Abstract

A continuum model for the growth of self-assembled quantum dots that incorporates surface diffusion, an elastically deformable substrate, wetting interactions and anisotropic surface energy is presented. Using a small slope approximation a thin film equation for the surface profile that describes facetted growth is derived. A linear stability analysis shows that anisotropy acts to destabilize the surface. It lowers the critical height of flat films and there exists an anisotropy strength above which all thicknesses are unstable. A numerical algorithm based on spectral differentiation is presented and simulation are carried out. These clearly show faceting of the growing islands and a logarithmically slow coarsening behavior.

Keywords: Anisotropic surface energy; self-assembly of quantum dots; linear stability; small-slope approximation; stationary solutions; coarsening

1 Introduction

Epitaxial growth of quantum dots is a fascinating topic from many points of view. The self-assembled patterning and the geometrical structure of the growing solid film inherits a natural beauty that alone may be worth studying (for pictures of dots see references [1, 6, 18, 25]). However, apart from the interest it may raise due to inherent structures and symmetries, the nano-crystals can be very valuable for industrial applications, because their semiconducting properties make them useful for electronic and optoelectronic devices. The blue laser is one of the main achievements which can be attributed to research on quantum dots [21]. LEDs with a wide color spectrum and a small energy consumption are under consideration and even quantum computing is of interest due to the two-state property of a quantum dot [17]. Recently the photovoltaic industry tries

*Weierstrass Institute for Applied Analysis and Stochastics (WIAS), D-10117 Berlin, Germany (korzec@wias-berlin.de).

†Institute for Mathematics, Humboldt University of Berlin, D-10099 Berlin, Germany (pevans@mathematik.hu-berlin.de).

to incorporate the zero-dimensional structures - or "artificial atoms" because of their discrete energy states - inside new thin layers in order to increase the thermodynamic conversion efficiency [22, 15]. For widespread applications, comparatively cheap, but controllable self-assembly growth processes are needed.

We concentrate on the most common material combination, germanium crystals grown on silicon (Ge/Si), for a review see Drucker [6] or the references therein. Atoms of germanium are deposited on top of the silicon substrate in a hot chamber (the effects we describe and simulate occur at about 500 degrees Celsius) and after a pseudomorphic growth phase the Asaro-Tiller-Grinfeld (ATG) instability [5] leads to formation of initially round structures (prepyramids) which in later stages morph to tiny pyramids, the quantum dots. Further deposition leads to multi-faceted domes and eventually dislocations that deteriorate the quality of the quantum dots.

A main mechanism for the growth is the lattice mismatch. Both crystalline materials have diamond cubic symmetry, but different lattice constants. The film is in the Stranski-Krastanov growth mode. In the first stage it adjusts its lattice to the prescribed width of the substrate's crystal structure inducing elastic energy that is competing with surface energy. In a layer by layer growth phase the surface remains flat, but as the film thickness increases strain energy can be released by the formation of quantum dots [28]. During the growth both materials undergo an deformation and the observed dots are faceted after primary forming more rounded prepyramids. Anisotropy is responsible for pyramidal shapes or multifaceted domes that are visible at later times. We consider only the anisotropy of the surface energy, though in principle also anisotropic elasticity coefficients may be significant (see recent work of Pang and Huang [23]).

Different methods are used to model and simulate the growth described above [7]. Stochastic methods that act on atomic scales are very accurate. However, only small domains with few dots can be simulated on short time-intervals. Monte Carlo simulations have been implemented, but are very time-consuming [16, 19]. To treat big domains for longer times, continuum models are used. For the mesoscopic description of the elasticity problem finite element methods allow for the solution of the Navier-Cauchy equations in three dimensions (e.g. Zhang et al. [37]). To avoid the high computational costs it is common to simplify the governing equations. A small slope approximation similar to lubrication theory in fluids is applied. For literature see Atherton and Davis [2].

Based on Mullins' diffusion model [20] many formulas incorporating different chemical potentials have been proposed. Spencer and co-workers derived partial differential equations without wetting or anisotropy [31, 30, 32]. Later Golovin et al. included wetting effects [13] and analyzed the linear stability of a more complete model [14]. However, for simulations of reduced models the important effects of stress and wetting were neglected. They used an anisotropy formula which Savina et al. incorporated as the main mechanism for the evolution together with normal growth from the vapor phase [27]. Inclusion of a cusped model for the anisotropic surface energy has been accomplished by Eisenberg and Kandel [8, 9, 10], who obtained promising 2D results. The anisotropy model

is different to others in that it uses a nonsmooth cusp for the minimum of the surface energy. This can be a drawback since methods based on derivatives will have problems with the numerical simulations.

Solving the elastic subproblem is one of the main tasks for the simulation of self-assembled growth. Instead of working with full Navier Cauchy equations on a 3D domain, we use solution approximations based on small-slope reduction. Pang and Huang [24] used the Cerruti solution for a semi-infinite solid that is subjected to a point force. The resulting leading order equation is qualitatively the same as the derived by Tekalign and Spencer [33, 34]. Here we present a consistent model reduction including anisotropy which results in a self-contained partial differential equation. We let the surface energy be dependent on orientation such that it has local minima at the facets of the dots. This has been also proposed by Chiu and Huang [4] who used a sum of exponentials depending on the surface's normals to describe preferred orientations. However, it is simple and sufficient to use a fourth order polynomial in the slopes of the surface in x and y directions. A model reduction via small-slope approximation leads to a self-contained PDE. Simulations show how surfaces initially roughen, then facet and coarsen on a logarithmically slow time-scale. The overall model we consider contains surface diffusion, linear elasticity, anisotropic surface energy and wetting interactions.

In the rest of our paper we present first in Section 2 the general equations for the model, such as a diffusion formula and terms of the chemical potential. We describe the elasticity problem and an anisotropy formula to obtain the full equation for the problem. Thereafter in Section 3 we use characteristic scales [33] to simplify the equations. In this way we derive our model in two and three dimensions and analyze it in Sections 4 and 5, respectively. The results of numerical simulations using a pseudospectral method are presented. Stationary states are computed as solutions of an ODE with a second method. These equal the shapes from long-run simulations of the PDE and show tent-like or pyramidal shapes which validates the correctness of the derivation of the evolution equation. A linear stability analysis extends the isotropic theory. It shows that the critical thickness of a flat film decreases and that the unstable regime grows with increasing anisotropy strength. Above a certain value an infinite range of wave numbers is unstable. Using long-time simulations with large numbers of pyramids we examine the logarithmic coarsening in two and three dimensions. The results are reviewed in the last Section where we also present an outlook for future plans.

2 Modeling the self-assembly of quantum dots

We consider the dislocation-free evolution of a thin solid film on a substrate as sketched in Fig. 1. We denote the position of the film surface with $z = h(x, y, t)$ at time t and a point in the periodic spatial domain (x, y). We will refer to this case as the three-dimensional one. Later the case when $h = h(x, t)$ will be referred to as two-dimensional. The interface between the materials is assumed

to be at $z = 0$.

Based on surface diffusion [20], in the absence of deposition the film evolution satisfies

$$h_t = \sqrt{1 + |\nabla h|^2}\, \mathcal{D} \nabla_s^2 \mu \tag{1}$$

with the diffusion constant $\mathcal{D} = \Omega^2 D_s \sigma / (kT)$. Here μ is the chemical potential, Ω is the atomic volume, σ the surface density of atoms, D_s the diffusion coefficient, k the Boltzmann constant and T the absolute temperature. The surface Laplacian is defined as

$$\nabla_s^2 = \frac{1}{N^2}((1 + h_y^2)\partial_{xx} + (1 + h_x^2)\partial_{yy} - 2h_x h_y \partial_x \partial_y - \kappa N(h_x \partial_x + h_y \partial_y)) \quad , \tag{2}$$

where $N = \sqrt{1 + \|\nabla h\|^2}$ and κ is the mean curvature [32]. It is chosen here to have a positive sign in case of a standard parabola that is bounded below,

$$\kappa = \frac{h_{xx}(1 + h_y^2) + h_{yy}(1 + h_x^2) - 2h_x h_y h_{xy}}{N^3} \quad . \tag{3}$$

We consider a chemical potential μ that consists of two terms

$$\mu = \mathcal{E}_{sed} + \mathcal{E}_{surf} \tag{4}$$

representing the competing contributions from elastic and surface energies, respectively. The first term is the strain energy density evaluated at the surface

$$\mathcal{E}_{sed} = \frac{1}{2}\sigma_{ij}\epsilon_{ij} \mid_{z=h} \tag{5}$$

with the stresses σ_{ij} and strains ϵ_{ij} related by Hooke's law. As usual in elasticity theory we use Einstein's notation and sum over repeated indices $i, j \in \{1, 2, 3\}$. The problem to be solved to compute the term (5) is described in Section 2.1 and follows Tekalign and Spencer [33].

The other term in (4) is decomposed into three components by taking the functional derivative of the surface free energy. The right-hand side of the following equation is defined via the calculation of this derivative.

$$\mathcal{E}_{surf} := \frac{\delta}{\delta h} \int \gamma(h, h_x, h_y) dS = \mathcal{E}_\kappa + \mathcal{E}_{wet} + \mathcal{E}_{anis} \quad . \tag{6}$$

The standard surface and wetting terms are

$$\mathcal{E}_\kappa = -\gamma\kappa \tag{7}$$

and

$$\mathcal{E}_{wet} = (\partial_h \gamma) n_3 \quad , \tag{8}$$

where $n_3 = 1/N$ is the third component of the outward unit normal. Since the surface energy also depends on orientation, an additional term arises

$$\begin{aligned} \mathcal{E}_{anis} = \quad & - \quad 2\left(\frac{h_x h_{xx} + h_y h_{xy}}{N} \partial_{h_x} \gamma + \frac{h_y h_{yy} + h_x h_{xy}}{N} \partial_{h_y} \gamma\right) \\ & - \quad N \partial_x (\partial_{h_x} \gamma) - N \partial_y (\partial_{h_y} \gamma) \,. \end{aligned} \tag{9}$$

Using a formula that depends only on the surface height, $\gamma = \gamma(h)$, such as Spencer's boundary layer formula [29] (see later in Section 2.2, formula (19)) gives formally the terms $\mathcal{E}_\kappa$ and $\mathcal{E}_{wet}$. Including the third term $\mathcal{E}_{anis}$ is vital to correctly model effects of surface energy anisotropy which is our main goal.

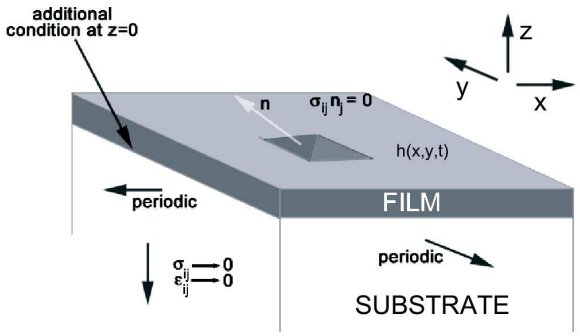

Figure 1: Epitaxy setting: a film of thickness h grows on a substrate occupying an infinite half-space.

2.1 The strain energy density

The lattice mismatch is crucial for the self-assembly of quantum dots and results in stresses in film and substrate. These are represented in the strain energy density (5) evaluated on the free surface. The displacements in all spatial dimensions are denoted by $u_i, i = 1, 2, 3$. Using linear elasticity the strains are the symmetric part of the displacement gradient tensor

$$(\epsilon_{ij})_{i,j\in\{1,2,3\}} = \frac{1}{2}(\nabla u + \nabla u^T) \tag{10}$$

and are related to the stress tensor by Hooke's law for isotropic materials

$$\sigma_{ij} = \frac{E}{1+\nu}\epsilon_{ij} + \frac{E\nu}{(1+\nu)(1-2\nu)}\epsilon_{kk}\delta_{ij} \quad i,j \in \{1,2,3\}\,. \tag{11}$$

Here ν is Poisson's ratio and E is the elastic modulus. Mechanical equilibrium is assumed to be reached on a much faster time-scale than the thermodynamic equilibrium. This condition requires

$$\nabla \cdot \sigma = 0 \quad , \tag{12}$$

and together with (10) and (11) results in the Navier-Cauchy equations of isotropic linear elasticity theory

$$(1-2\nu)\Delta u + \nabla(\nabla \cdot u) = 0 \quad . \tag{13}$$

Once boundary conditions are defined and the displacements are computed, one obtains the strains, the stresses and finally the strain energy density using (5).

At the film free surface we assume the pressure to be negligible, so that there the boundary condition is

$$\sigma \cdot n = 0 \quad \text{at} \quad z = h \quad . \tag{14}$$

Deep inside the substrate the stresses vanish, so that

$$u_i^s \to 0 \quad \text{for } z \to -\infty \quad . \tag{15}$$

Throughout the document we use superscript f to indicate a quantity belongs to the film and s if it is related to the substrate. The origin of variables without superscripts are supposed to be known from the context, so that most of the time they may be omitted.

At the interface between the two crystalline materials it is assumed that the displacements of the film are equal to those of the substrate with an additional correction in x and y directions arising from lattice mismatch

$$u_i^f = u_i^s + \epsilon[x, y, 0]^T \quad \text{at} \quad z = 0 \quad , \tag{16}$$

where the lattice mismatch parameter $\epsilon = (a^f - a^s)/a^f$. Here a^s and a^f are the lattice spacings in the substrate and in the film, respectively.

As last condition continuity of the stress tensor at the film-substrate interface is necessary

$$\sigma^f_{|z=0} = \sigma^s_{|z=0} \quad . \tag{17}$$

The elasticity problem is governed by the equations (11)-(17).
For a flat film that has adjusted its lattice spacing to that of the undeformed substrate, one can easily compute the strain energy density

$$\mathcal{E}_{sed}^{base} = \frac{E^f}{1 - \nu^f}\epsilon^2 \quad . \tag{18}$$

However $\mathcal{E}_{sed}$ is more difficult to derive for non-flat surfaces. When the ratio of thickness to characteristic spatial length is small, this parameter allows for asymptotic expansions of the displacements. This model reduction will be discussed in Section 3.

2.2 Anisotropic surface energy

Spencer [29] proposed a boundary layer model for the smooth transition of the surface energy from the substrate's value to the film's

$$\gamma(h) = \frac{1}{2}(\gamma^f + \gamma^s) + (\gamma^f - \gamma^s)\frac{1}{\pi}\arctan(h/b) \quad , \tag{19}$$

where b is the transition length scale and $\gamma^p, p \in \{f, s\}$ are material constants. We generalize (19) by letting γ^f be anisotropic, but leave the surface energy density of the substrate unchanged, hence isotropic. We let γ^f depend on the slopes

of the surface such that we can assign different energies to different orientations of the free surface

$$\gamma(h, h_x, h_y) \quad = \quad \frac{1}{2}(\gamma^f(h_x, h_y) + \gamma^s) + (\gamma^f(h_x, h_y) - \gamma^s)\frac{1}{\pi}\arctan(h/b) \,. \tag{20}$$

We use a simple formula for the anisotropic surface energy

$$\gamma_f(h_x, h_y) = \gamma_0(1 + \mathcal{W}(h_x, h_y)) \quad . \tag{21}$$

Here $\mathcal{W}$ could be chosen in various ways. Chiu and Huang [4] applied a sum of exponentials that defines minima at prescribed orientations. We choose a simpler, though less flexible model, a 'double double-well'

$$\mathcal{W}(h_x, h_y) = \tilde{G}(h_x^4 + h_y^4) - 2G(h_x^2 + h_y^2), \quad \tilde{G}, G > 0 \quad , \tag{22}$$

that could be extended to arbitrary polynomials in the lateral derivatives of the free surface. However, this function will be sufficient to describe the pyramidal structures with $\{1\,0\,5\}$ facets of quantum dots observed in experiments [6]. These define a characteristic slope s. For a flat film it has the value γ_0 and we will choose the dimensionless, positive parameters G and $\tilde{G}$ such that (21) has minima at $(\pm s, s), (s, \pm s)$ and a local maximum at $(0, 0)$. Other orientations that are not preferred are punished by the character of the polynomial, as $\gamma_f \to \infty$ for $h_x, h_y \to \pm\infty$.

The terms $\partial_{h_x}\gamma$ and $\partial_{h_y}\gamma$ appearing in the chemical potential (9) can be obtained easily

$$\nabla_{\nabla_h}\gamma := \begin{pmatrix} \partial_{h_x} \\ \partial_{h_y} \end{pmatrix}\gamma \quad = \quad \gamma_0\Psi(b, h)\nabla_{\nabla_h}\mathcal{W} \quad , \tag{23}$$

with the transition function

$$\Psi(b, h) = \frac{1}{2} + \frac{1}{\pi}\arctan(h/b) \quad , \tag{24}$$

and the derivative

$$\nabla_{\nabla_h}\mathcal{W} = 4\begin{pmatrix} \tilde{G}h_x^3 - Gh_x \\ \tilde{G}h_y^3 - Gh_y \end{pmatrix} \quad . \tag{25}$$

At this point we have obtained all equations that define a full model for the evolution of self-assembled quantum dots. However, since the displacements, which define stress and strain and hence the strain energy density (5), are given only as solution of a 3D elasticity problem, the whole system is hardly solvable without reducing it to simpler equations. A popular method to do so is using characteristic scales to identify small terms that can be neglected.

3 Thin-film scaling

Drucker [6] reports that pyramidal Ge/Si quantum dots have $\{1\,0\,5\}$ facets before before they start to become dome-like and create dislocations. Hence the

horizontal length scale (the base length of a facet) is large in comparison to the vertical scale (its height). The crystals have small slopes which can be used to neglect small terms - such as powers of gradients - in the evolution equation. If H_0 is a small characteristic thickness scale and L is a bigger scale for the substrate directions x and y, then the parameter $\alpha = H_0/L \ll 1$ can be used for asymptotic expansions [30, 33]. A generic scaling of the variables is

$$h = H_0 H = \alpha L H,\ z = \alpha L Z,\ (x, y) = (LX, LY)$$
$$t = \tau T,\ u_i(x, y, z) = L U_i(X, Y, Z) \quad .$$

Furthermore we scale the transition thickness

$$b = L\alpha^3 \bar{b} \quad , \tag{26}$$

so that the leading order of the wetting term $\mathcal{E}_{wet}$ will be of the same order as the surface energy term $\mathcal{E}_\kappa$. To guarantee that the overall reduced leading order PDE that we will derive is well posed in terms of the anisotropy, the double-well character of the anisotropy must remain in the leading order term of $\mathcal{E}_{anis}$. Therefore we assume

$$G = \mathcal{O}(1) \quad \text{and} \quad \tilde{G} = G/\alpha^2 \quad ,$$

such that $\mathcal{W} = \alpha^2 W$ with

$$W(H_X, H_Y) := G[(H_X^4 + H_Y^4) - 2(H_X^2 + H_Y^2)] \quad . \tag{27}$$

These assumptions correspond to the theory from Chiu and Huang [3] who chose the minimum of the facets to be only 1.2% smaller than γ_0.

We choose the characteristic length and time scales

$$L = \frac{\gamma_0}{\mathcal{E}_{sed}^{base}} \quad \text{and} \quad \tau = \frac{L^4}{\mathcal{D}\gamma_0} \quad , \tag{28}$$

respectively. These result from the nondimensionalization of the chemical potential

$$\mu = \frac{\gamma_0}{L}\bar{\mu}, \quad \bar{\mu} = \bar{\mathcal{E}}_{sed} + \bar{\mathcal{E}}_\kappa + \bar{\mathcal{E}}_{wet} + \bar{\mathcal{E}}_{anis} \tag{29}$$

which arises from the natural scalings

$$\sigma_{ij} = \mathcal{E}_{sed}^{base}\bar{\sigma}_{ij},\ \kappa = L\bar{\kappa},\ \gamma = \gamma_0\gamma,\ \nabla_s^2 = L^2\bar{\nabla}_s^2 \quad . \tag{30}$$

The evolution equation (1) in nondimensional form becomes

$$H_T = \sqrt{1 + \alpha^2(H_X^2 + H_Y^2)}\,\bar{\nabla}_s^2(\bar{\mathcal{E}}_{sed} + \bar{\mathcal{E}}_\kappa + \bar{\mathcal{E}}_{wet} + \bar{\mathcal{E}}_{anis}) \quad , \tag{31}$$

The constituent terms are

$$\begin{aligned}
\bar{\mathcal{E}}_{sed} &= \frac{1}{2}\bar{\sigma}_{ij}\epsilon_{ij} \\
\bar{\mathcal{E}}_{\kappa} &= -\bar{\gamma}\bar{\kappa} \\
\bar{\mathcal{E}}_{wet} &= \frac{(\gamma_f - \gamma_s)\alpha\bar{b}}{\gamma_0\pi(\alpha^4\bar{b}^2 + H^2)\sqrt{1+\alpha^2\|\nabla H\|^2}} \qquad (32) \\
\bar{\mathcal{E}}_{anis} &= -2\alpha\frac{(H_X H_{XX} + H_X H_{XY})\partial_{H_X}\mathcal{W} + (H_Y H_{YY} + H_Y H_{XY})\partial_{H_Y}\mathcal{W}}{(1+\alpha^2(H_X^2+H_Y^2))^{1/2}} \qquad (33) \\
&\quad -\frac{1}{\alpha}(1+\alpha^2(H_X^2+H_Y^2))^{1/2}\left(\partial_X\left[\Psi\partial_{H_X}\mathcal{W}\right] + \partial_Y\left[\Psi\partial_{H_Y}\mathcal{W}\right]\right),
\end{aligned}$$

where in the last expression we used the transition function with rescaled arguments $\Psi = \Psi(L\alpha^3\bar{b}, H_0 H)$.

Now we expand the nondimensionalized chemical potential

$$\bar{\mu} = \bar{\mu}^{(0)} + \alpha\bar{\mu}^{(1)} + \mathcal{O}(\alpha^2)$$

and determine the leading order terms. Derivative operators such as the nabla operator $\nabla = (\partial_X, \partial_Y)^T$ or the Laplacian $\Delta = \nabla^2$ are from now on defined in the new variables. The surface Laplacian $\bar{\nabla}_s^2$ can be expanded

$$\bar{\nabla}_s^2 = \Delta + \mathcal{O}(\alpha^2) \qquad (34)$$

so that to order α the evolution equation can be written as

$$H_T = \Delta(\bar{\mu}^{(0)} + \alpha\bar{\mu}^{(1)}). \qquad (35)$$

The aim of the following paragraphs will be to derive the leading order terms of the chemical potential that can be inserted into the above equation (35).

The strain energy density terms $\bar{\mathcal{E}}_{sed}^{(0)}, \bar{\mathcal{E}}_{sed}^{(1)}$:
With expansions for the strains and stresses

$$\bar{\sigma}_{ij} = \bar{\sigma}_{ij}^{(0)} + \alpha\bar{\sigma}_{ij}^{(1)} + \alpha^2\bar{\sigma}_{ij}^{(2)} + \mathcal{O}(\alpha^3), \quad \epsilon_{ij} = \epsilon_{ij}^{(0)} + \alpha\epsilon_{ij}^{(1)} + \alpha^2\epsilon_{ij}^{(2)} + \mathcal{O}(\alpha^3) \qquad (36)$$

one can find an expansion for the strain energy density

$$\bar{\mathcal{E}}_{sed} = \bar{\mathcal{E}}_{sed}^{(0)} + \alpha\bar{\mathcal{E}}_{sed}^{(1)} + \mathcal{O}(\alpha^2) \quad . \qquad (37)$$

By using (36) and the Navier-Cauchy equations in the film and substrate one obtains

$$\bar{\mathcal{E}}_{sed}^{(0)} = 1 \quad \text{and} \quad \bar{\mathcal{E}}_{sed}^{(1)} = \mathcal{F}^{-1}(-eku) \qquad (38)$$

with $k = \sqrt{k_1^2 + k_2^2}$ the length of the wave vector (k_1, k_2) which is composed of the wave numbers k_1 and k_2 for two dimensions, and where

$$e = \frac{2\mu^f(1+\nu^f)(1-\nu^s)}{\mu^s(1-\nu^f)} \quad . \qquad (39)$$

Here $\mu^p = E^p/(2(1+\nu^p)), p \in \{f, s\}$ is the shear modulus of film and substrate, respectively, and u denotes the 2D Fourier transform $\mathcal{F}(H)$. Its inverse is

$$H(X,Y,T) = \mathcal{F}^{-1}(u) = \int\limits_{[-\infty,\infty]^2} u(k_1,k_2,T) e^{-ik_1X - ik_2Y} dk_1\, dk_2\,.$$

A detailed derivation of these terms is given by Tekalign and Spencer [33].

The surface energy terms $\bar{\mathcal{E}}_\kappa^{(0)}, \bar{\mathcal{E}}_\kappa^{(1)}$:
The curvature can be expanded in terms of α to

$$\bar{\kappa} \quad = \quad \alpha\bar{\kappa}^{(1)} + \mathcal{O}(\alpha^3) \tag{40}$$

with the leading order coefficient

$$\bar{\kappa}^{(1)} = \Delta H \quad . \tag{41}$$

This gives

$$\bar{\mathcal{E}}_\kappa \quad = \quad -\left\{\frac{1}{2}\frac{\gamma_0+\gamma^s}{\gamma_0} - \frac{\tilde{\gamma}}{\bar{b}}\arctan\left(\frac{H}{\alpha^2\bar{b}}\right)\right\}\bar{\kappa}^{(1)}\alpha + \mathcal{O}(\alpha^3) \tag{42}$$

$$= \quad -\alpha\bar{\kappa}^{(1)} + \mathcal{O}(\alpha^2) \quad , \tag{43}$$

with $\tilde{\gamma} = \bar{b}(\gamma_0 - \gamma^s)/(\gamma_0\pi)$, where typically $\tilde{\gamma} > 0$, so that a film covering the substrate is favorable. We derived

$$\bar{\mathcal{E}}_\kappa^{(0)} = 0 \quad \text{and} \quad \bar{\mathcal{E}}_\kappa^{(1)} = -\Delta H \tag{44}$$

and remark that the anisotropy does not have any influence on the surface term $\bar{\mathcal{E}}_\kappa$ to leading order.

The wetting energy terms $\bar{\mathcal{E}}_{wet}^{(0)}, \bar{\mathcal{E}}_{wet}^{(1)}$:
For the expansion of the wetting term

$$\bar{\mathcal{E}}_{wet} = \bar{\mathcal{E}}_{wet}^{(0)} + \alpha\bar{\mathcal{E}}_{wet}^{(1)} + \mathcal{O}(\alpha^2) \tag{45}$$

the coefficients are determined by expanding (32) to

$$\bar{\mathcal{E}}_{wet} \quad = \quad \alpha\frac{\tilde{\gamma}}{H^2}\left(1 - \frac{\alpha^2\|\nabla H\|^2}{2}\right) + \mathcal{O}(\alpha^4) \quad .$$

We read off the wetting coefficients

$$\mathcal{E}_{wet}^{(0)} = 0 \quad \text{and} \quad \mathcal{E}_{wet}^{(1)} = -\frac{\Delta\gamma}{LH^2} \quad . \tag{46}$$

The anisotropy terms $\bar{\mathcal{E}}_{anis}^{(0)}, \bar{\mathcal{E}}_{anis}^{(1)}$:
Finally we also expand the anisotropy term

$$\bar{\mathcal{E}}_{anis} = \bar{\mathcal{E}}_{anis}^{(0)} + \alpha\bar{\mathcal{E}}_{anis}^{(1)} + \mathcal{O}(\alpha^2) \tag{47}$$

and determine the leading order expressions. Therefore we expand the fractions and the transition function in (33)

$$\begin{aligned}\bar{\mathcal{E}}_{anis} = & - 2\alpha(1-\alpha^2\frac{H_X^2+H_Y^2}{2})(1-\alpha^2\frac{\bar{b}}{H})\left\{(H_XH_{XX}+H_XH_{XY})\partial_{H_X}\mathcal{W}\right. \\ & + \left.(H_YH_{YY}+H_YH_{XY})\partial_{H_Y}\mathcal{W}\right\}+\mathcal{O}(\alpha^3) \\ & - \frac{1}{\alpha}(1+\alpha^2\frac{H_X^2+H_Y^2}{2})\left(\partial_X\left[(1-\alpha^2\frac{\bar{b}}{H})\partial_{H_X}\mathcal{W}\right]+\partial_Y\left[(1-\alpha^2\frac{\bar{b}}{H})\partial_{H_Y}\mathcal{W}\right]\right).\end{aligned}$$

Due to our choice of $\mathcal{W}$ (27), the lowest order of this expression is

$$\alpha\bar{\mathcal{E}}^{(1)}_{anis} = -\frac{1}{\alpha}\nabla\cdot\nabla_{\nabla H}\mathcal{W}(H_X,H_Y) = -\alpha\nabla\cdot\nabla_{\nabla H}W(H_X,H_Y) \quad . \quad (48)$$

The reduced evolution equation:
Using $\Delta\mu^{(0)}=0$ the evolution equation (35) becomes

$$H_T = \Delta(\bar{\mathcal{E}}^{(1)}_{sed}+\bar{\mathcal{E}}^{(1)}_{\kappa}+\bar{\mathcal{E}}^{(1)}_{wet}+\bar{\mathcal{E}}^{(1)}_{anis}). \quad (49)$$

Insertion of the derived terms (38), (44), (46) and (48) into (49) gives the final evolution equation

$$H_T = \Delta[\mathcal{F}^{-1}(-eku)-\Delta H-\frac{\tilde{\gamma}}{H^2}-\nabla\cdot\nabla_{\nabla H}W(H_X,H_Y)] \quad (50)$$

The character of the above PDE is changed from semilinear in the isotropic case $G=0$ to quasilinear when $G>0$ and it is well-posed as long as G is below a certain threshold that is determined in the linear stability analysis part. It will be presented in the next Section together with the numerical method for the two-dimensional case and results on stationary solutions and coarsening.

4 Evolution in one lateral and one time dimension (2D)

Now we consider only one lateral dimension X, so that the film is described by $H=H(X,T)$. Here island profiles represent long parallel ridges in 3D. Evolution equation (50) then simplifies to

$$H_T = \partial_{XX}[\mathcal{F}^{-1}(-e|k|u)+(4G-12GH_X^2-1)H_{XX}-\frac{\tilde{\gamma}}{H^2}] \quad . \quad (51)$$

The elasticity term is reduced from (38), where $k=\sqrt{k_1^2+k_2^2}\geq 0$. Note that now $k=k_1$ is a wave number in one dimension and we have to take its absolute value inside the inverse Fourier transform. We see, qualitatively the isotropic model [33] is extended by adding one nonlinear term $\partial_{XX}[H_X^2H_{XX}]$. Simulations may be carried out with the following semi-implicit method.

4.1 The numerical method

We simulate equation (51) using a pseudospectral method. In Fourier space, with $u = \mathcal{F}(H)$, the evolution equation becomes

$$u_T = -k^2(-e|k|u + k^2 u - \tilde{\gamma}\mathcal{F}[\frac{1}{H^2}] - ik\mathcal{F}[w'(H_X)]) \quad (52)$$

$$= \mathcal{L}(u) + k^2\mathcal{N}(k, H, H_X) \quad (53)$$

with the linearity

$$\mathcal{L}(u) = \mathcal{L}u = (ek^2|k| + (4G-1)k^4)u \quad (54)$$

and the nonlinearity

$$\mathcal{N}(k, H, H_X) = 4Gik\mathcal{F}(H_X^3) + \tilde{\gamma}\mathcal{F}[\frac{1}{H^2}]\,.$$

For a backward Euler scheme with implicitly treated linear term, explicit nonlinearity and the discrete vectors $U \in \mathbb{R}^n \approx u(k)_{k\in\mathcal{K}}$, $\mathcal{K}$ is a set of wave numbers, the fast Fourier transform (FFT) is used to compute $\mathcal{N}$ and its inverse to plot the surfaces. The update scheme is

$$U^+(k) = \frac{U(k) - \Delta t k^2 \mathcal{N}}{1 - \Delta t \mathcal{L}}\,, \quad k \in \mathcal{K}\,, \quad (55)$$

where superscript + indicates the new time-step. We were able to analyze stationary shapes of single quantum dots and the coarsening behavior of large arrays of two-dimensional dots - or ridges/wires - with a *Matlab* code.

For our simulations we take material constants corresponding to a germanium film on a silicon substrate. For Ge we use $\mu_f = 0.41\times10^5$ J/cm^3, $\nu_f = 0.27$, $\gamma_0 = 0.19 \times 10^{-5}$ J/cm^2 [33] and for the Si substrate $\mu_s = 0.80 \times 10^5$ J/cm ^{3}, $\nu_s = 0.28$, [36]. The characteristic length in this system is $L \approx 8$ nm. The resulting elasticity parameter $e = 2\mu_f(1+\nu_f)(1-\nu_s)/(\mu_s(1-\nu_f)) \approx 1.28$, and the wetting parameter $\tilde{\gamma} = 0.05$.

4.2 Linear stability analysis and stationary solutions

A linear stability analysis of equation (51) with the normal mode ansatz

$$H = \bar{H} + \delta e^{\sigma t + ikX}$$

for $\delta \ll \bar{H}$ gives the characteristic equation

$$\sigma = (4G-1)k^4 + ek^2|k| - \frac{2\tilde{\gamma}}{\bar{H}^3}k^2 \quad (56)$$

for the growth of small disturbances to a uniform film of thickness $\bar{H}$. This dispersion relation is plotted in Fig. 2. We remark that it is valid for more arbitrary polynomials than (22), so that this result holds also for a more general case. Two

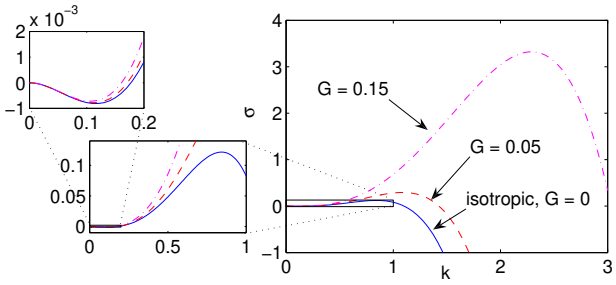

Figure 2: Dispersion relation for the isotropic ($G = 0$) and the anisotropic cases $G = 0.05$ and $G = 0.15$ with $\bar{H} = 0.8$. On the left we see a magnifications of the wave number regime where the minimum is adopted.

stable regimes surround an unstable interval of wave lengths as in the isotropic case. However, we see that the parameter G dictates the sign of the highest power of the polynomial (56). For growing values of $G \in (0,\, 1/4)$ the maximal value is attained at larger wave lengths and higher modulus. Anisotropy destabilizes any flat film if G is strong enough as indicated in Fig. 3. Bigger values of the anisotropy decrease the critical height

$$H_c = H_c(G) = 2\left(\frac{\tilde{\gamma}(1-4G)}{e^2}\right)^{1/3}$$

below which all films are stable (Fig. 3 on the right). Further for each anisotropy strength there is a critical wave number k_c above which the film is stable

$$k_c = k_c(G) = \frac{e}{1-4G} \quad .$$

Since $k_c \to \infty$ for $G \to 1/4$ (Fig. 3, left), films are unstable above this critical anisotropy strength for an infinite range of wave numbers.

A uniform film of thickness $\bar{H}$ is unstable for a range of wave numbers less than k_c. This relation is described in Fig. 3 (left) and we observe that the stability region grows with decreasing G. For the above parameter, in the isotropic case $H_c(0) = 0.63$ and for the anisotropic values it decreases to $H_c(0.05) = 0.58$ and $H_c(0.15) = 0.46$, respectively. During a slow epitaxial deposition process we anticipate growth of pyramids shortly after the deposited film exceeds this critical thickness.

Fig. 4 shows results of a typical simulation, starting from an initial profile $H(X, 0) = 0.7$, plus a small random perturbation with amplitude 0.0001 on a domain of length 4π. By $t = 15$ the perturbations have grown somewhat, forming three oscillations. They merge to form two islands, separated by a wetting layer, by $t = 50$. These show distinct facets, surfaces with relatively constant slope $H_X \approx \pm 1$. At longer times, they collapse to form a single faceted island. By $t = 200$ the numerical method produces film profiles which are

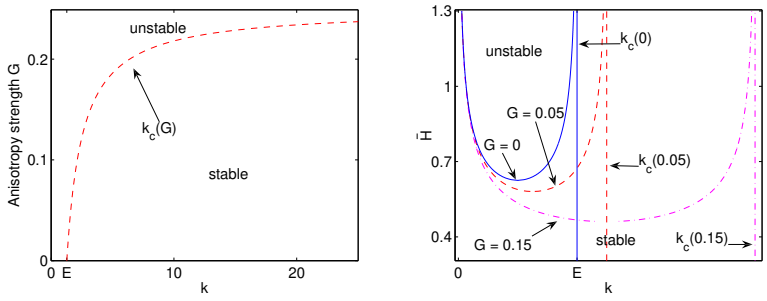

Figure 3: Stability regime plots, left: varying anisotropy strength versus wave numbers depicting $k_c(G)$ as dashed line. By increasing G the unstable region grows and becomes infinite for $G = 0.25$; right: stability diagram for $G = 0, G = 0.05$ and $G = 0.15$ and varying k and $\bar{H}$. The vertical lines are the corresponding values of the critical wave number $k_c(G)$.

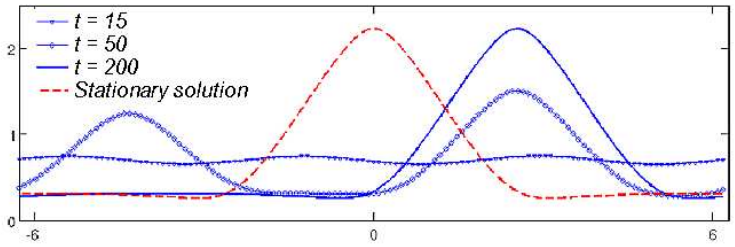

Figure 4: Evolution of a solid film governed by (51) from a nearly-uniform initial profile and anisotropy strength $G = 0.1$. At long times, triangular shaped islands form, collapse, and the shifted profile approaches that given by the steady state solution described in Section 4.2 (dashed curve).

stationary in the sense that successive iterates H_k and H_{k+1} differ by less than a small threshold δ times the time step

$$\frac{\|H_{k+1} - H_k\|}{\|H_k\|} < \delta \Delta t \quad .$$

The long-time profiles may be compared to the steady solutions obtained by setting $H_T = 0$ in (51). In this case the chemical potential is a constant, μ_0, so that

$$-H_{XX} - e\mathcal{F}^{-1}(|k|\mathcal{F}(H)) - \frac{\tilde{\gamma}}{H^2} - \mathcal{F}^{-1}(ik\mathcal{F}(w'(H_X))) = \mu_0 \qquad (57)$$

with $w'(H_X) = 4G(H_X^3 - H_X)$ being the derivative of the one-dimensional double-well. We solve (57) using a pseudospectral approach in which a Newton-type method is used to satisfy (57) at each mesh point. We treat the value

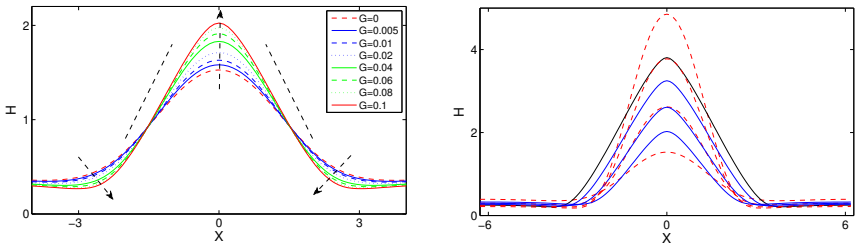

Figure 5: Steady profiles for periodic solutions. (a) Increasing surface energy anisotropy strength G, with fixed film volume V. (b) Increasing V from $V = 2.6\pi$ to $V = 4.8\pi$; for $G = 0.1$, leads to a family of facetted islands (solid lines). With constant surface energy, width remains approximately constant (dashed lines).

of μ_0 as an unknown, assume periodic boundary conditions, and impose the additional requirements that the volume of the film is fixed, that is,

$$\int_0^L H \, \mathrm{d}X = V = \bar{H} L \tag{58}$$

where $\bar{H}$ is a constant. Furthermore the solution is supposed to be symmetric around $X = 0$.

In Fig. 4 a solution to (57) is shown for the same parameters as in the time-dependent solution obtained by the scheme (55). The agreement is very good, with the time dependent solution being a translation of the stationary shape. These results were computed with $N = 128$ mesh points; results for $N = 64$ and $N = 256$ are almost indistinguishable, indicating the convergence of the method under mesh refinement.

We explored the effect of the anisotropy strength by computing stationary profiles for G between 0 and 0.1, shown in Fig. 5(a). The islands develop a more faceted appearance for larger values of G. As G increases, the sides of the islands take on slopes closer to ± 1, corresponding to the minima of the one-dimensional version of W in (27).

We then fixed $G = 0.1$ and increased the film volume. The resulting family of steady profiles are shown in Fig. 5(b) for V from 2.6π to 4.8π. For constant film surface energy ($G = 0$), islands have approximately constant width as V increases [26, 33]; For the largest volume profile shown there the free surface slopes are up to 2.7. For $G > 0$ the family of shapes are significantly different; instead as V increases, the island base widens, while the wetting layer region shrinks. Slopes remain moderate, reaching 1.33 for $V = 1.2L$. This family of "tent-like" solutions is more representative of real quantum dot behavior as dots grow while preserving their facets.

4.3 Coarsening behavior

We studied coarsening of large two-dimensional quantum dot arrays using (55). Simulations began with small random perturbations of a flat state above the critical thickness of the film. On a grid with 2048 points and time-steps $\Delta t = 0.0001$ for the Ge/Si system parameters we observed a behavior that is already indicated by the computed stationary solutions from the previous Section. The disturbance grows into many small rounded humps that are connected by a thin layer. They morph into faceted islands that are similar to those presented in Section 4.2. Bigger islands survive and retain a faceted form, while smaller ones are "eaten". One such run is visualized in Fig. 6, where again brighter shades are bigger film thicknesses. We can see the Ostwald ripening process (survival of the fattest) and collapses of dots. Although in early stages some of the structures tend to approach each other, no real collisions between islands are observed. Before they collide they collapse - they are absorbed by the thin film. The evolution plotted in Fig. 6 reminds us of coarsening in liquid films [12].

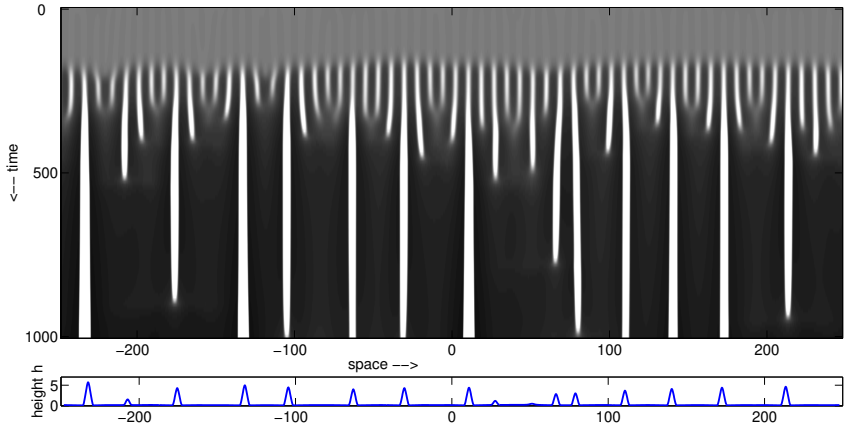

Figure 6: Simulation of coarsening of the 2D Ge/Si system. White shades correspond to thicker regions. Below the shape $H(X, 500)$ at $T = 500$ is shown. It corresponds to a line one would draw in the above black and white plot through the same time point.

With the presented pseudospectral method we analyzed coarsening rates. Therefore we use the value $<N>=<N>(t)$ which is the island density at time t - here this is the number of dots divided by the domain length parameter M for a domain of length $2\pi M$. We average the number of dots over four different runs for the isotropic case $G = 0$ and the two anisotropy strengths $G = 0.05$ and $G = 0.15$. The results are shown in Fig. 7 where the time on a logarithmic scale is plotted against the characteristic density number $<N>$. There appear to be two phases in the evolution, one where the island-structures form - being

larger for smaller values of G - and a second where actually coarsening takes place. Surface energies that depend on orientation lead to more islands in the first stage of evolution. This is confirmed by the linear stability analysis from the last Section which has shown that for bigger values of G the most unstable wave number increases. For $G = 0.15$ the fast coarsening regime sets in nearly instantly, while in the isotropic case this coarsening phase happens at much later times. Once dots start to collapse, isotropic coarsening is faster than for non-zero values of G. At long times the number of dots decreases like $-\log(t)$. This differs from power-law behavior $< N > \sim t^{-\beta}, \beta \in \mathbb{Q}_+$ seen in somewhat similar liquid systems [12]. However, Cahn-Hilliard type systems describing binary systems of solid materials may display logarithmic coarsening at late time [35].

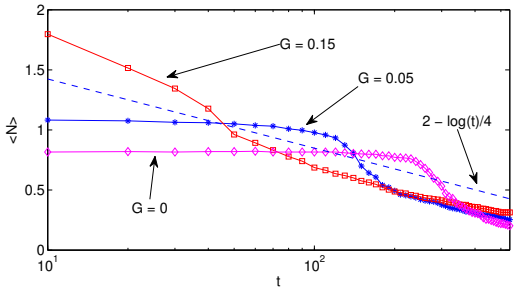

Figure 7: Coarsening diagram for the 2D Ge/Si system comparing dot densities for the isotropic ($G = 0$) and two anisotropic trials ($G = 0.05$ and $G = 0.15$). One trial is the average of four runs and the t-axis is logarithmic.

5 Surface evolution in 3D

In this Section we first explain the changes one has to apply to the pseudospectral method presented before to approximately solve the 3D evolution equation (50). The free surface depends again on two lateral variables X and Y, so that $H = H(X, Y, T)$. We then discuss the results obtained with this method - typical Ostwald ripening behavior and coarsening of faceted nano-islands. Numerical simulations can be carried out in the same manner as in Section 4.1, extended to two lateral dimensions. Equation (50) in Fourier space becomes

$$u_T \quad = \quad \mathcal{L}(u) + k^2 \mathcal{N}(k_1, k_2, H, H_X, H_Y) \tag{59}$$

with the formally unchanged linearity (54) and nonlinearity

$$\mathcal{N}(k_1, k_2, H, H_X, H_Y) = ik_1 \mathcal{F}[4GH_X^3] + ik_2 \mathcal{F}[4GH_Y^3] + \tilde{\gamma} \mathcal{F}[\frac{1}{H^2}] \ .$$

For a FFT-based spectral implementation with a backward Euler scheme with implicitly treated linear term, explicit nonlinearity and the discrete vectors $U \approx$

u, we use update formula (55), where instead of k the pair (k_1, k_2) serves as argument. As before we use parameters for the Ge/Si system and two different anisotropy strengths G.

5.1 3D results

In Fig. 8 we show the collapse of a dot. Two initially Gaussian humps close-by each other with different sizes first evolve to small pyramids. Higher regions are denoted by whiter shades and flat regions are colored black. Contour lines help to visualize how they change from round to nearly squared as an effect of the anisotropy. The smaller pyramid is "eaten" by $T = 15$, its material is absorbed by the thin layer, and only one bigger faceted quantum dot remains. Again this is reminiscent of Ostwald ripening which is well studied for different problems.

In Fig. 9 a surface is monitored from above during evolution with the same

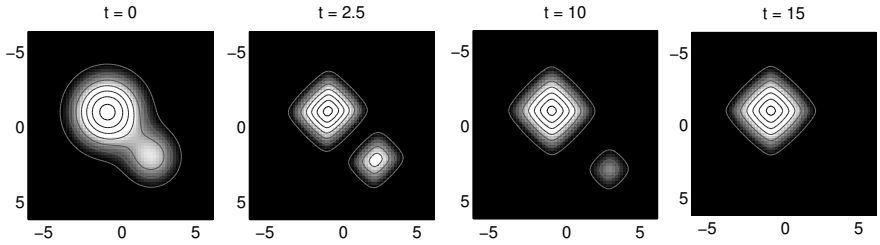

Figure 8: Collapse of a Ge/Si dot. Bright colors show bigger values of the surface height. The initial condition for these two islands were two round, exponential humps that initially evolve to faceted structures. The bigger quantum dot "eats" the smaller one and survives. The simulation has been carried out with $G = 0.2$. Time and space are given here and in the other figures in dimensionless units.

color to surface height relation as before. An initially flat film was perturbed by small random noise with mean zero. Initially ridge-like structures form that are more pronounced for larger G. These evolve to arrays of round dots that are connected through a thin layer. After some time the faceting sets in. Bigger dots have a faceted shape resembling the pyramids seen in experiments for the Ge/Si system [6], or also for the GeSi films on Si [11].

As in the 2D case stronger anisotropy parameters lead to more oscillatory surfaces in the first stages and the facets are more pronounced. A linear stability analysis as in Section 4.2 for the 3D equation leads to qualitatively the same result of a growing interval of unstable wave numbers for larger values of G. The initial perturbations evolve to surfaces with higher spatial frequencies and result in more small dots. Fig. 10 visualizes the effect of anisotropy. At the same point in time simulations results for $G = 0, G = 0.1$ and $G = 0.25$ are plotted. A few dots are enlarged for $G = 0$ and $G = 0.25$ to accent the effect of anisotropy. For the bigger value of G the facets are sharper and also the small islands have more rectangular bases.

To analyze coarsening rates, we computed solutions on a $n \times n$ grid with $n = 256$ and used the measure

$$< N >=< N > (t) = \frac{N(t)}{M^2}$$

for monitoring the dot density. Here $N(t)$ is the number of dots at time t and M is the domain length in one dimension divided by 2π. In Fig. 11 we see, that the

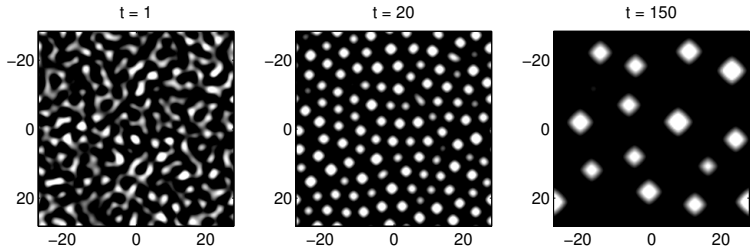

Figure 9: Simulation of the Ge/Si system. An initially randomly perturbed surface first evolves into round dots that coarsen in time and during their growth change their shape to small pyramids.

onset of coarsening is fast and behaves proportional to $-\log(t)$ for a nonzero value of G. The curve for the isotropic case $G = 0$ shows that after formation of a bumpy surface nothing happens in early stages of evolution. Once coarsening sets in, it is faster than with anisotropy. It seems that the lower energy state for faceted islands slightly stabilizes the islands.

6 Summary and outlook

We presented a partial differential equation that properly describes the evolution of self-assembled quantum dots above a critical thickness. It was obtained by incorporation of a surface diffusion formula and a chemical potential that includes terms from linear elasticity, anisotropic surface energy and intermolecular forces at the film-substrate interface. A consistent small slope reduction results in self-contained evolution equations in two and three dimensions. It extends the model from Tekalign and Spencer [33] by anisotropic surface energy, which enters as an additional nonlinear term. Our numerical studies show that this nonlinearity can sufficiently model the anisotropy. The structure of the term - a double well slope-potential in two dimensions - allows for an efficient numerical implementation based on spectral differentiation.

We investigated stationary solutions in two dimensions confirming the faceted shapes resulting from long runs of the PDE simulations. It is also observed during the logarithmically slow coarsening, be it in two or three dimensions. As a result of the linear stability analysis, stronger anisotropy leads in early times to creation of more dots. These coarsen slower than in the isotropic model once

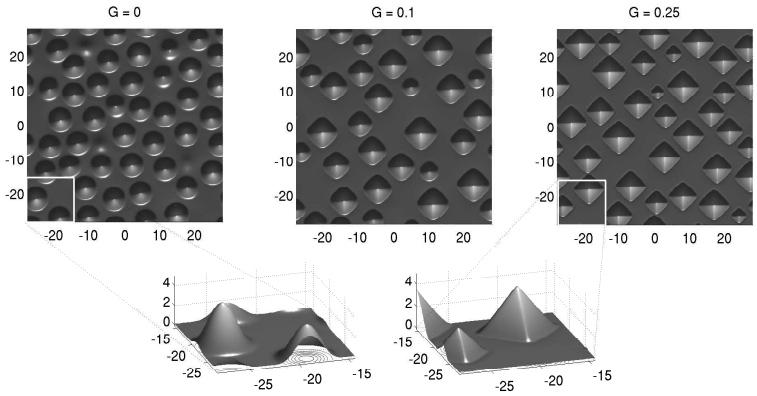

Figure 10: Anisotropy effect on the 3D Ge/Si system. All three pictures show the same time-point after evolution from the same initial condition (random perturbation of a flat state). The upper left shows a simulation with isotropic surface tension ($G = 0$) and the dots have round tips. In the other two pictures ($G = 0.1$ and $G = 0.25$) we observe faceting which is stronger for the bigger anisotropy coefficient G.

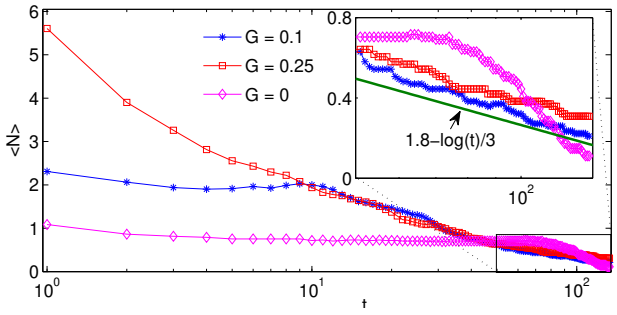

Figure 11: Coarsening diagram for the 3D case. No ($G = 0$), weak ($G = 0.1$) and strong ($G = 0.25$) anisotropy. The solid line is the negative logarithm of the time with a vertical shift. The t-axis is in log scale.

there the coarsening regime is reached. More systematic studies on stationary solutions and coarsening rates are ongoing. Another challenge that has not been addressed here is the addition of an atomic flux to the evolution equations. For realistic simulations of epitaxial growth this must not be neglected for comparison with experiments.

Acknowledgment

This work was performed as part of Project C-10 of the DFG research center MATHEON, Berlin. Both authors thank B. Wagner and A. Münch for fruitful discussions, proposals for improving this manuscript and their support.

References

[1] K. Alchalabi, D. Zimin, G. Kostorz, and H. Zogg. Self-assembled semiconductor quantum dots with nearly uniform sizes. *Phys. Rev. Lett.*, 90:026101–4, 2003.

[2] R. W. Atherton and G. M. Homsy. On the derivation of evolution equations for interfacial waves.

[3] C.-H. Chiu and Z. Huang. Common features of nanostructure formation induced by the surface undulation on the Stranski-Krastanow systems. *Appl. Phys. Lett.*, 89:171904, 2006.

[4] C.-H. Chiu and Z. Huang. Numerical simulation for the formation of nanostructures on the Stranski-Krastanow systems by surface undulation. *J. Appl. Phys.*, 101:113540, 2007.

[5] A. Danescu. The Asaro-Tiller-Grinfeld instability revisited. *Int. J. of Solids and Structures*, 38:4671–4684, 2001.

[6] J. Drucker. Self-Assembling Ge(Si)/Si(001) Quantum Dots. *IEEE J. Quantum Electronics*, 38(8):975–987, 2002.

[7] A. Voigt (editor). *Multiscale Modeling in Epitaxial Growth.* Birkhauser, 2005.

[8] H. R. Eisenberg and D. Kandel. Wetting layer thickness and early evolution of epitaxially strained thin films. *Phys. Rev. Lett.*, 85(6):1286–1289, 7 August 2000.

[9] H. R. Eisenberg and D. Kandel. Origin and properties of the wetting layer and early evolution of epitaxially strained thin films. *Phys. Rev. B*, 66:155429, October 2002.

[10] H. R. Eisenberg and D. Kandel. Formation, ripening, and stability of epitaxially strained island arrays. *Phys. Rev. B*, 71:115423, 2005.

[11] J. A. Floro, E. Chason, R. D. Twesten, R. Q. Hwang, and L. B. Freund. SiGe coherent islanding and stress relaxation in the high mobility regime. *Phys. Rev. Lett.*, 79(20):3946–3949, November 1997.

[12] K. B. Glasner and T. P. Witelski. Coarsening dynamics of dewetting films. *Phys. Rev. E*, 67(1):016302, January 2003.

[13] A. A. Golovin, S. H. Davis, and P. W. Voorhees. Self-organization of quantum dots in epitaxially strained solid films. *Phys. Rev. E*, 68:056203, 2003.

[14] A. A. Golovin, M. S. Levine, T. V. Savina, and S. H. Davis. Faceting instability in the presence of wetting interactions: A mechanism for the formation of quantum dots. *Phys. Rev. B*, 70:235342, 2004.

[15] J. Konle, H. Presting, and H. Kibbel. Self-assembled Ge-islands for photovoltaic applications. *Physica E*, 16(3-4):596–601, 2003.

[16] C.-H. Lam, C.-K. Lee, and L. M. Sander. Competing Roughening Mechanisms in Strained Heteroepitaxy: A Fast Kinetic Monte Carlo Study. *Phys. Rev. Lett.*, 89(21):216102, 2002.

[17] D. Loss and D. P. DiVincenzo. Quantum computation with quantum dots. *Phys. Rev. A*, 57(1):120–126, Jan 1998.

[18] G. Medeiros-Ribeiro, A. M. Bratkovski, T. I. Kamins, D. A. A. Ohlberg, and R. S. Williams. Shape Transition of Germanium Nanocrystals on a Silicon (001) Surface from Pyramids to Domes. *Science*, 279(5349):353–355, 1998.

[19] M. Meixner, E. Schoell, V. A. Shchukin, and D. Bimberg. Self-assembled quantum dots: Crossover from kinetically controlled to thermodynamically limited growth. *Phys. Rev. Lett.*, 87(23):1–4, 2001.

[20] W. W. Mullins. Theory of thermal grooving. *J. Appl. Phys.*, 28(3):333–339, March 1957.

[21] S. Nakamura, G. Fasol, and S.J. Pearton. *The Blue Laser Diode: The Complete Story*. Springer, 2000.

[22] A. J. Nozik. Quantum dot solar cells. *Physica E*, 14(1-2):115–120, 2002.

[23] Y. Pang and R. Huang. Effect of elastic anisotropy on surface pattern evolution of epitaxial thin films. *accepted in Int. J. Solids and Structures.*

[24] Y. Pang and R. Huang. Nonlinear effect of stress and wetting on surface evolution of epitaxial thin films. *Phys. Rev. B*, 74:075413, 2006.

[25] F. M. Ross, R. M. Tromp, and M. C. Reuter. Transition states between pyramids and domes during Ge/Si island growth. *Science*, 286(5446):1931–1934, 3 December 1999.

[26] C. D. Rudin and B. J. Spencer. Equilibrium island ridge arrays in strained solid films. *J. Appl. Phys.*, 86(10):5530–5536, 15 Nov 1999.

[27] T. V. Savina, A. A. Golovin, S. H. Davis, A. A. Nepomnyashchy, and P. W. Voorhees. Faceting of a growing crystal surface by surface diffusion. *Phys. Rev. E*, 67:021606, 2003.

[28] V. A. Shchukin and D. Bimberg. Strain-driven self-organization of nanostructures on semiconductor surfaces. *Appl. Phys. A*, 67:687–700, 1998.

[29] B. J. Spencer. Asymptotic derivation of the glued-wetting-layer model and contact-angle condition for Stranski-Krastanow islands. *Phys. Rev. B*, 59(3):2011–2017, January 1999.

[30] B. J. Spencer, S. H. Davis, and P. W. Voorhees. Morphological instability in epitaxially strained dislocation-free solid films: Nonlinear evolution. *Phys. Rev. B*, 47(15):9760–9777, April 1993.

[31] B. J. Spencer, P. W. Voorhees, and S. H. Davis. Morphological instability in epitaxially strained dislocation-free solid films. *Phys. Rev. Lett.*, 67(26):3696–3699, December 1991.

[32] B. J. Spencer, P. W. Voorhees, and S. H. Davis. Morphological instability in epitaxially strained dislocation-free solid films: Linear stability theory. *J. Appl. Phys.*, 73(10):4955–4970, 1993. Part 1, May 15.

[33] W. T. Tekalign and B. J. Spencer. Evolution equation for a thin epitaxial film on a deformable substrate. *J. Appl. Phys.*, 96(10):5505–5512, 2004.

[34] W. T. Tekalign and B. J. Spencer. Thin-film evolution equation for a strained solid film on a deformable substrate: Numerical steady states. *J. Appl. Phys.*, 102:073503, 2007.

[35] S. J. Watson, F. Otto, B. Rubinstein, and S. H. Davis. Coarsening dynamics of the convective Cahn-Hilliard equation. *Phys. D*, 178:127–148, 2003.

[36] J. J. Wortman and R. A. Evans. Young's modulus, shear modulus, and poisson's ratio in silicon and germanium. *J. Appl. Phys.*, 36(1), 1965.

[37] Y. W. Zhang, A. F. Bower, L. Xia, and C. F. Shih. Three dimensional finite element analysis of the evolution of voids and thin films by strain and electromigration induced surface diffusion. *J. Mech. Phys. Sol.*, 47(1):173–199, 4 December 1998.